Electron collisions with the NO_2 radical using the *R*-matrix method

Hema Munjal,[1] K. L. Baluja,[1] and Jonathan Tennyson[2]
[1]*Department of Physics and Astrophysics, University of Delhi, Delhi 110007, India*
[2]*Department of Physics and Astronomy, University College London, London WC1E6BT, United Kingdom*
(Received 30 March 2008; published 20 March 2009)

The *R*-matrix method is used to calculate the elastic integral, differential, momentum transfer cross sections, and the excitation cross sections from the ground state $X\ ^2A_1$ to the five low-lying electronically excited states $A\ ^2B_1$, $B\ ^2B_2$, $C\ ^2A_2$, $^4A_2$, and $^4B_2$ of the NO_2 radical. Twenty-one target states are included in the close-coupling expansion of the scattering system, where each target state is represented by configuration-interaction wave function. The calculations give two shape resonances of $^3B_1$ and $^1B_1$ symmetries located at 1.18 and 2.33 eV, respectively, with a common configuration $6a_1\ 2b_1$. We also detect eight core-excited shape resonances and one Feshbach resonance. Partial elastic, total, and electronic excitation cross sections are presented and compared with the limited previous work. The dissociative nature of the $^3B_1$ and $^1B_1$ shape resonances is explored by performing scattering calculations in which one N-O bond is stretched while the other bond and the bonding angle are frozen. These resonances support dissociative attachment yielding NO and O^- in their respective ground states.

DOI: 10.1103/PhysRevA.79.032712 PACS number(s): 34.80.Bm, 34.80.Ht, 34.80.Gs

I. INTRODUCTION

Electron-molecule collisions are of fundamental importance and have many useful applications for the modeling of discharges in low-temperature gases, laser physics, atmospheric and interstellar models, isotope separation, radiation physics, and magneto-hydro dynamics power generation. The design of plasma reactors is still based on empirical studies due to lack of reliable cross sections for the excitation and dissociation pathways in reactive gases employed in plasma processing. The accurate simulation of electron-molecule scattering at low scattering energies remains a computational challenge.

The nitrogen dioxide molecule plays an important role in modeling atmospheric processes [1]. It is a trace constituent in the atmosphere but there is an increase in its emission rate caused by human activity. The chemiluminescence process known as "air afterglow" is of interest to aeronomists; in this process ground-state nitric oxide molecules and oxygen atoms recombine causing emission from excited states of NO_2. The radical NO_2 like other radicals (NO, OH, and HO_2) strongly affects the ozone concentration in the atmosphere by converting O_3 to O_2.

We make a brief review of the existing knowledge of the relevant work on NO_2 radical. Due to a variety of applications, its spectroscopy has been studied in great detail in recent years. It has been known that its visible and near-infrared spectra are very complex due to various perturbations among the electronic states. The low-lying states $A\ ^2B_1$ and $B\ ^2B_2$ lie in this energy range. Earlier bound-state calculations [2] were carried out for the low-lying electronic states of NO_2 molecule using multiconfiguration self-consistent wave functions. It has been shown [3] that the excited state $B\ ^2B_2$ and the ground state $X\ ^2A_1$ couple nonadiabatically to form a strongly coupled pair of $2A'$ states when asymmetric distortion of the bond lengths is considered. The geometry of the $C\ ^2A_2$ state has been studied in detail using coupled-cluster theory with large basis sets [4]. Potential-energy surfaces of the $X\ ^2A_1$, $A\ ^2B_1$, and $B\ ^2B_2$ electronic states and the transition dipole moment surfaces of the transitions $X\ ^2A_1$-$A\ ^2B_1$ and $X\ ^2A_1$-$B\ ^2B_2$ have been computed [5] using complete active space self-consistent field (CASSCF) and internally contracted multireference configuration-interaction (IC-MRCI) methods.

The study of photonic and electronic collisions with NO_2 has also attracted great attention. Several studies of NO_2 photoionization have been performed [6–8]. Stephan *et al.* [9] studied single and double ionizations of NO_2 by electron impact from threshold up to 180 eV and Benoit and Abouaf [10] studied vibrational excitation of NO_2 by low-energy ($<$2.5 eV) electron impact. Experiments [11–13] have also probed negative-ion formation by electron dissociative attachment of NO_2. Absolute total cross sections for electron collisions from NO_2 were measured by Szmytkowski *et al.* [14] using a linear beam transmission experiment at collision energies from 0.6 to 220 eV. Curik *et al.* [15] presented new calculations of the integral elastic cross sections for electron scattering from NO_2 in the ground electronic state using a single-center expansion (SCE) method at the static-exchange (SE) level with addition of a model correlation-polarization potential. However, their study made no allowance for electronic excitation processes.

In this work, we report on elastic integral, elastic differential, momentum transfer, and excitation cross sections for electron impact on NO_2 radical. These calculations are performed using the UK polyatomic *R*-matrix code [16,17]. This method can provide a good description of the electron correlations in several excited states of the molecule [18].

II. OUTLINE OF THE *R*-MATRIX METHOD

The main idea of the *R*-matrix method is the partitioning of the coordinate space into an inner region and an outer region. These regions are separated by a spherical boundary of radius *a*. The center of mass of the molecule defines the origin of the coordinate system. The *R*-matrix radius is cho-

sen so that it envelops the entire charge cloud of all the target electronic states included in the calculation. In the inner region, the scattering electron is indistinguishable from the electrons of the target making the problem hard but solvable. When the scattering electron is at large distances from the target, where there is no residual molecular charge density, exchange interactions with any of the target electron can be neglected, which greatly simplifies the problem in the outer region.

In the inner region, the wave function is written using the configuration-interaction (CI) expression

$$\Psi_k^{N+1} = A\sum_{ij} \Phi_i^N(x_1, \ldots, x_N)\xi_j(x_{N+1})a_{ijk} + \sum_m \chi_m(x_1, \ldots, x_N, x_{N+1})b_{mk}, \quad (1)$$

where A is an antisymmetrization operator, x_N is the spatial and spin coordinates of the Nth electron, Φ_i^N represents the ith state of the N-electron target, ξ_j is a continuum orbital spin coupled with the target wave function. The sum in the second term of the above expression represents short-range polarization effects; it runs over configurations χ_m, where all $(N+1)$ electrons are placed in target occupied and virtual molecular orbitals. These are described as the L^2 configurations and are also important for relaxing the orthogonality imposed between the target and continuum orbitals. Coefficients a_{ijk} and b_{mk} are variational parameters determined by diagonalization of the Hamiltonian matrix. The quantity Φ_i^N represents the N-electron target and the summation in the first term generates "target+continum" configurations.

In this calculation, the target molecular orbital space is divided into core (inactive), valence (active), and virtual orbitals. These target molecular orbitals are supplemented with a set of continuum orbitals, centered on the center of mass of the molecule. The continuum basis functions, used in polyatomic R-matrix calculations, are Gaussian functions and do not satisfy fixed boundary conditions [16]. First, target and continuum molecular orbitals are orthogonalized using a Schmidt orthogonalization procedure, then symmetric or Löwdin orthogonalization is used to orthogonalize continuum molecular orbitals among themselves and remove linearly dependent functions [16,19].

III. NO_2 ELECTRONIC STATES

Our calculations on NO_2 used the double zeta plus polarization (DZP) Gaussian basis set (9,5,1)/(4,2,1) of Dunning and Hay [20] for nitrogen and oxygen atoms. We supplemented the DZP set with an extra d function with an exponent of 0.2 on both N and O atoms. This supplemented set was further augmented with two f functions with exponents of 0.2 and 0.8 for N and with exponents of 0.2 and 0.85 for O. The Hartree-Fock configuration of the ground state $X\ ^2A_1$ of NO_2 molecule is (core) $(4a_1^2\ 5a_1^2\ 3b_2^2\ 1b_1^2\ 4b_2^2\ 1a_2^2\ 6a_1)$. The core represents ten electrons in the orbitals $1b_2$, $1a_1$, $2a_1$, $3a_1$, and $2b_2$, which are doubly occupied. The SCF energy for the ground state using the present basis set is −204.0707 a.u. and the dipole moment is 0.738 D at the experimental geometry [5] where the N-O bond length is 1.194 Å and the ONO angle is 133.86°. The energies of the highest occupied molecular orbitals of the $1b_1$, $4b_2$, $1a_2$, and $6a_1$ irreducible representations (IRs) are −20.54, −14.86, −14.24, and −6.85 eV, respectively. The first two unoccupied orbitals are $2b_1$ and $7a_1$ which have energies of 2.52 and 11.04 eV, respectively. In our CI model, we freeze ten electrons in the core and the remaining 13 electrons are free to occupy the $4a_1$, $5a_1$, $6a_1$, $7a_1$, $1b_1$, $2b_1$, $3b_2$, $4b_2$, and $1a_2$ orbitals. In this CI model, the energy of the ground state is lowered to −204.144 54 a.u. and the dipole moment is decreased to 0.455 D, which is in fair agreement with the experimental value of 0.316 D [21]. The ground-state quadrupole components Q_{20} and Q_{22} are −0.699 and −1.871 a.u., respectively, in our CI model.

We found no R-matrix poles in the $^1A_1$ scattering symmetry with an energy below that of the ground state $X\ ^2A_1$, which indicates that there is no bound state of the anion NO_2^-. Experimentally, however, this state is bound with (adiabatic) electron affinity of 2.27 eV [22]. It is imperative to get an accurate estimate of vertical electron affinity (VEA) because the existence of a strongly bound negative ion may have profound effects on the behavior of cross sections for the corresponding scattering symmetry. It is known that NO_2^- supports a bound state for its ground electronic configuration. We have attempted to induce more correlation effects in $^1A_1$ scattering symmetry by performing SCF calculation on the ground state $^1A_1$ of NO_2^- at the NO_2 equilibrium geometry. This SCF calculation indicated that the highest occupied molecular orbital (HOMO) $6a_1$ is bound by 1.93 eV, which according to Koopman's theorem gives the value of VEA. The lowest pole, of $^1A_1$ symmetry, using SCF orbitals of NO_2^- is −204.159 a.u. which is lower than the ground-state energy of NO_2 state, thus making this anionic state bound. The modified SCF orbitals were then used for the $^1A_1$ symmetry. Our partial cross sections for $^1A_1$ symmetry are in good agreement with the SCE calculations in the energy region considered here. The modified SCF orbitals for $^1A_1$ symmetry are used for static-exchange and close-coupling calculations.

We now describe the dominant configurations of the low-lying excited states. The excited state $A\ ^2B_1$ arises due to the promotion of an electron from the occupied $6a_1$ orbital to an unoccupied $2b_1$ orbital whereas the excited state $B\ ^2B_2$ arises due to the promotion of an electron from the doubly occupied $4b_2$ orbital to the singly occupied $6a_1$ orbital leaving a hole in the $4b_2$ orbital. The excitation of an electron from $1a_2$ to $6a_1$ orbital gives rise to the $C\ ^2A_2$ electronic state. The quartet states $^4A_2$ and $^4B_2$ have configurations $4b_26a_12b_1$ and $1a_26a_12b_1$, respectively. The vertical excitations energies of the doublet and quartet states calculated using our CI model are presented in Table I and are compared with the other theoretical results. The excitation energy of $A\ ^2B_1$ state in our CI model is 3.08 eV which is in good agreement with the CASSCF [5] value of 3.02 eV; however, our corresponding value for the $B\ ^2B_2$ state is higher by 0.60 eV than the CASSCF value. The excitation values for the remaining states are compared with the older multiconfiguration SCF calculation of Gillispie *et al.* [2] as CASSCF values are not available for these states. There is good agreement between

TABLE I. Vertical excitation energies (in eV) and transition moments (in a.u.) of NO_2 using our CI model at the experimental geometry.

Symmetry No.	State	Present work (eV)	Transition dipole moment (a.u.)	Previous work (eV)
1	$X\ ^2A_1$	0.00	0.1791	0.00
2	$^2B_1$	3.08	0.0757	3.02 [5]
3	$^2B_2$	4.03	0.2081	3.43 [5]
4	$^2A_2$	4.07	0.0000	3.40 [2]
5	$^4A_2$	4.99	0.0000	4.70 [2]
6	$^4B_2$	5.04	0.0000	4.60 [2]
7	$^2A_2$	5.96	0.0000	
8	$^2B_2$	6.27	0.2250	
9	$^2A_2$	7.33	0.0000	
10	$^2B_1$	8.19	0.1630	
11	$^2A_1$	8.21	0.0213	
12	$^2B_2$	8.83	0.7260	
13	$^4B_1$	9.29	0.0000	
14	$^2B_2$	9.84	0.0283	
15	$^2A_1$	9.86	0.0008	
16	$^2B_1$	10.25	0.1087	
17	$^4A_2$	10.81	0.0000	
18	$^2A_2$	10.81	0.0000	
19	$^2B_1$	10.83	0.0532	
20	$^4A_2$	12.10	0.0000	
21	$^2A_1$	12.21	0.0316	

our CI values and the multiconfiguration SCF values for the quartet states, which are nearly degenerate. For the $C\ ^2A_2$ state our value is higher by 0.67 eV. It is possible to increase the correlation in our CI model, thereby improving the excitation energies, but the scattering calculation becomes intractable.

IV. SCATTERING MODEL

We carried out the scattering calculations in SE and 21-state models. In SE model, only the ground state is included in the close-coupling expansion. The SE model neglects all target relaxation effects. However a few target virtuals are included; these provide orbitals for shape resonances. This model does not include polarization and/or correlation effects due to electronically closed channels.

The static-exchange calculations were used to assign the configuration of the shape and core-excited shape resonances. These calculations included some carefully chosen configurations, which allowed us to give orbital designations to the resonances that we found.

Our CI calculations used the 21 target states given in Table I in the close-coupling expansion [see Eq. (1)]. Calculations were performed for singlet and triplet states with A_1, B_1, B_2 and A_2 symmetries. Gaussians centered at the molecule center of gravity represented the continuum orbitals.

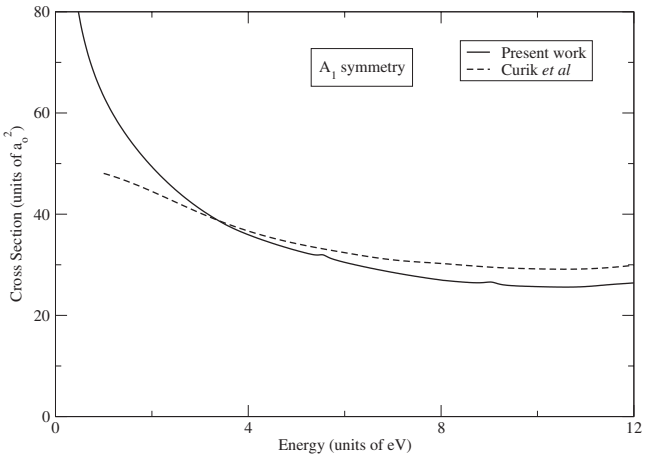

FIG. 1. 21-state R-matrix partial (up to l=4) cross section for the A_1 symmetry with NO_2^- SCF orbitals: solid curve, summed (singlet+triplet) and dashed curve, Curik *et al.* [15].

For this, the orbitals of Faure *et al.* [23] were used. Our calculations were performed for the continuum orbitals up to g partial waves. These continuum orbitals were orthogonalized to the target orbitals retained in the calculation and those with an overlap of less than 2×10^{-7} were removed [16]. It is important to preserve the balance between the amount of correlation included in the target states and in the scattering calculation. This is achieved by allowing 14 electrons (13 valence electrons +1 scattering electron) to move freely among $4a_1$, $5a_1$, $6a_1$, $7a_1$, $1b_1$, $2b_1$, $3b_2$, $4b_2$, and $1a_2$ molecular orbitals.

V. RESULTS

A. Elastic scattering

Due to the presence of a long-range dipole interaction, the elastic cross section is formally divergent in the fixed-nuclei approximation. However, since the dipole moment is small, its effect on the cross sections is expected to be small for

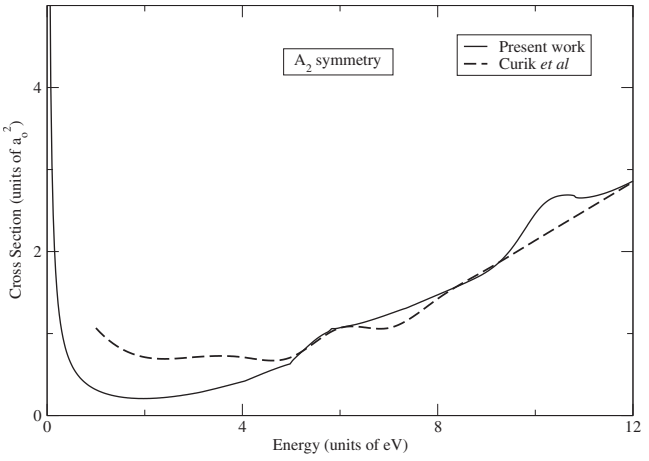

FIG. 2. 21-state R-matrix partial (up to l=4) cross section for the A_2 symmetry with NO_2 SCF orbitals: solid curve, summed (singlet+triplet) and dashed curve, Curik *et al.* [15].

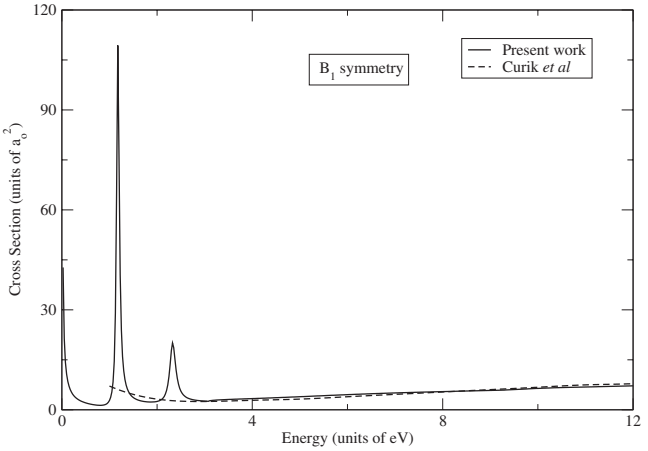

FIG. 3. Same as Fig. 2 but for the B_1 symmetry.

energies below 1 eV. There are four IRs A_1, A_2, B_1, and B_2 that contribute to the scattering process. Figures 1–4 compare the partial (up to l=4) cross sections (the sum of the singlet and triplet contributions) for these IR components calculated in the 21-state close-coupling model with the static-exchange values calculated by Curik *et al.* [15] who employed SCE of Gianturco and Lucchese [24]. In this SCE exchange effects are introduced through a separable exchange kernel and correlation-polarization effects are included via a model potential [24,25] calculated using density-functional theory [26]; long-range polarization was included via the experimental spherical dipole polarizability.

In Fig. 1, we have compared the partial elastic cross sections for the A_1 symmetry with the SCE results. Beyond 2 eV, the two curves are in fair agreement with each other. Figure 2 shows partial cross sections for A_2 symmetry. The magnitude of the A_2 cross sections is small compared to those of the other symmetries. There is qualitative agreement with the SCE results of Curik *et al.* [15]. The *R*-matrix calculations exhibit smooth behavior up to 10 eV. Figure 3 shows the partial cross sections of B_1 symmetry where we detect two resonances in the *R*-matrix results. These resonances also appear in the SE calculation but at higher energies. In the nonresonant energy regions we have good agreement with the SCE results. The two shape resonances are of $^1B_1$ and $^3B_1$ symmetries. By fitting the eigenphase sums to the Breit-Wigner form [27] we found that these resonances are located at 2.33 and 1.178 eV, respectively, with the corresponding widths of 0.15 and 0.083 eV. These resonances have a common configuration $6a_1\,2b_1$. Curik *et al.* [15] reported a single-particle resonance of b_1 orbital symmetry positioned at 2.21 eV calculated using a coupled adiabatic potential. This resonance reported by Curik *et al.* [15] is not visible in cross sections since it arises only in a separate adiabatic local potential calculation. This position agrees approximately with 1.75 eV, the average value of the positions of singlet and triplet components of B_1 symmetry found in the *R*-matrix calculation. This average position is close to energy for which there is an appearance of an O^- peak in the dissociative electron attachment spectra of NO_2 molecule [28].

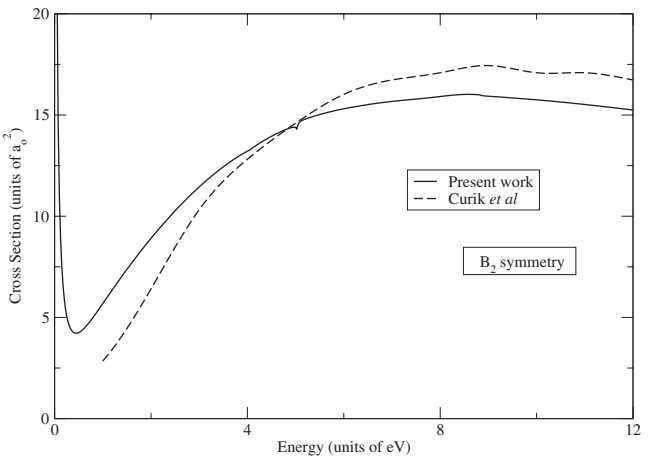

FIG. 4. Same as Fig. 2 but for the B_2 symmetry.

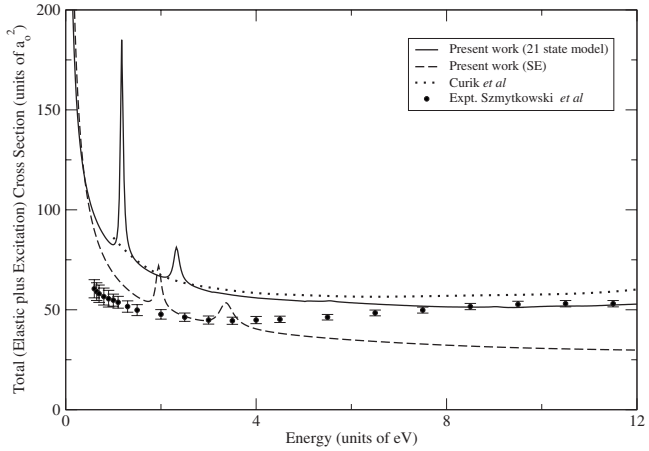

FIG. 5. Total (elastic plus excitation) cross sections for electron impact on NO_2: solid curve, *R* matrix (21-state model); dashed curve, static-exchange model; dotted curve, Curik *et al.* [15]; and circles, experiment of Szmytkowski *et al.* [14].

The partial cross sections of B_2 symmetry are displayed in Fig. 4 and show fair agreement with SCE calculation. For all the four IRs considered here the contribution of the triplet component is higher than the singlet contribution

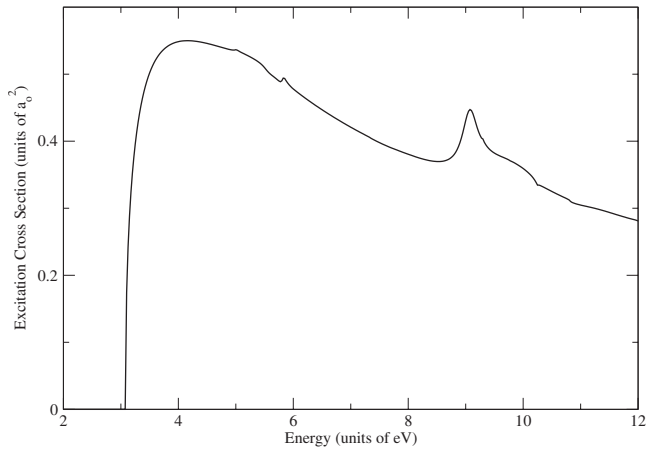

FIG. 6. 21-state *R*-matrix excitation cross section for the transition $X\ ^2A_1$-$A\ ^2B_1$.

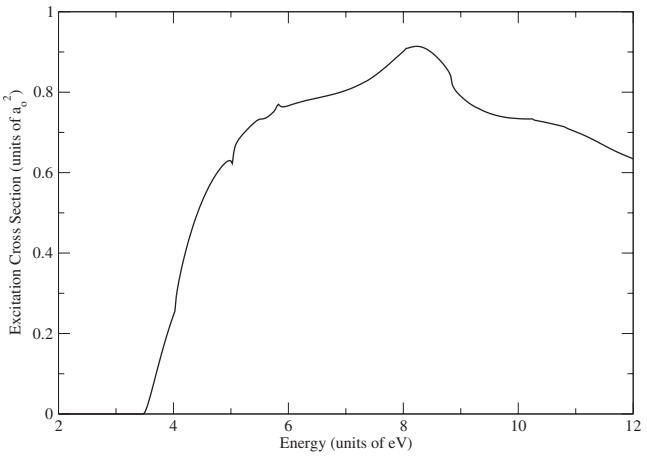

FIG. 7. 21-state *R*-matrix excitation cross section for the transition $X\ ^2A_1$-$A\ ^2B_2$.

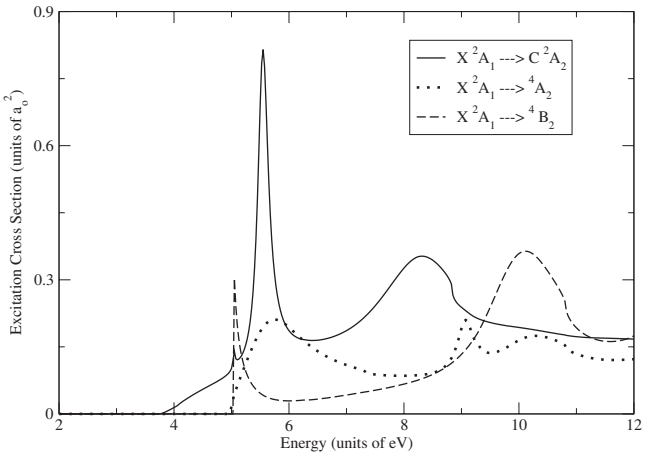

FIG. 8. 21-state *R*-matrix electron-impact excitation cross section: solid curve, $X\ ^2A_1$-$A\ ^2A_2$; dotted curve, $X\ ^2A_1$-$^4A_2$; and dashed curve, $X\ ^2A_1$-$^4B_2$.

Figure 5 presents the total (elastic and excitation) cross sections and the results are compared with previous theoretical [15] and experimental [14] studies. Since the vertical ionization potential of NO_2 is 11.23 eV [8], the contribution of ionization cross sections to the total cross sections is negligible for scattering energies below 12 eV. The *R*-matrix calculation results are in good agreement with the theoretical results of Curik *et al.* [15] for all energies. Beyond 5 eV, we also obtain good agreement with the experiment. For energies lower than 5 eV our cross sections are higher than the experiment and show resonance structures not found experimentally. It is typical that the observed cross section for electron impact on polar molecules is lower than the *ab initio* theoretical models at low energies. This is associated with difficulty of extrapolating experimental differential cross sections (DCSs) at low angles [29].

B. Excitation cross sections

Figures 6–8 present electron impact excitation cross sections from the ground state to the first five excited states using our 21-state scattering model. Transition moments from the ground state to the excited states are given in Table I. According to optical dipole selection rules, only the $X\ ^2A_1$-$A\ ^2B_1$ and $X\ ^2A_1$-$B\ ^2B_2$ transitions are allowed. A Born correction is employed for these transitions to account for higher partial waves neglected in the *R*-matrix calculation that takes only partial waves up to $l=4$ [30].

Figure 6 presents our excitation cross sections from the ground state to the allowed $A\ ^2B_1$ state. The sharp rise near threshold is due to the $^1B_1$ symmetry, which also dominates over other singlet components. The prominent feature around 9 eV is due to the $^3A_1$ symmetry. We also detect weaker features in the cross section for this excited state. These features correlate to the positions of core-excited resonances which are listed in Table II. Core-excited shape resonances are those that appear above the corresponding parent excited states of the molecule.

By manipulating the active space of the scattering calculation it is possible to assign shape resonances but not the core-excited shape resonances. For this case a bound-state

TABLE II. Anionic states of NO_2.

Symmetry No.	Symmetry	Designation of resonance	Type of resonance	Resonance position E_r (eV)	Parent state	Position of parent state (eV)
1	$^3B_1$	$6a_1\ 2b_1$	Shape	1.178	$X\ ^2A_1$	0.0
2	$^1B_1$	$6a_1\ 2b_1$	Shape	2.33	$X\ ^2A_1$	0.0
3	$^3B_2$	$1a_2^{-1}\ 6a_1^2\ 2b_1$	Core excited	5.1	$^2A_2$	4.07
4	$^3A_2$	$4b_2^{-1}\ 6a_1^2\ 2b_1$	Core excited	5.32	$^2B_2$	4.03
5	$^1A_1$	$6a_1^0\ 2b_1\ 2b_1$	Feshbach	5.57	$^2B_1$	8.19
6	$^1A_2$	$4b_2^{-1}\ 6a_1^2\ 2b_1$	Core excited	5.84	$^2B_2$	4.03
7	$^3B_2$	$4b_2^{-1}\ 6a_1^2\ 7a_1$	Core excited	8.3	$^2B_2$	4.03
8	$^1B_2$	$1a_2^{-1}\ 6a_1^2\ 2b_1$	Core excited	8.34	$^2A_2$	4.07
9	$^3A_1$	$1b_1^{-1}\ 6a_1^2\ 2b_1$	Core excited	9.1	$^2B_1$	3.08
10	$^3A_2$	$3b_2^{-1}\ 6a_1^2\ 2b_1$	Core excited	9.8	$^2A_2$	4.07
11	$^1A_2$	$3b_2^{-1}\ 6a_1^2\ 2b_1$	Core excited	10.2	$^2A_2$	4.07

calculation on the anionic states using the same CI model as for the corresponding neutral molecular states provides roots, which can be correlated with the positions of resonances found in the scattering calculation. We performed a similar calculation for the anionic states of NO_2 molecule and found that the resonance around 9 eV is a core-excited shape resonance with configuration $1b_1^{-1}\,6a_1^2\,2b_1$ in which the electron in the orbital $2b_1$ is dissociated leaving the target in the excited electronic state $A\ ^2B_1$. Resonance centered at 9.1 eV is also detected during excitation to the $^4A_2$ state (Fig. 8).

The cross sections for excitation to the $B\ ^2B_2$ state are shown in Fig. 7. This dipole-allowed transition has a larger cross section than the $X\ ^2A_1$-$A\ ^2B_1$ as its dipole transition moment is almost twice as large. The peak around 8 eV is due to the $^3B_2$ core-excited shape resonance at 8.3 eV (see Table II). The structures in the cross section in the 5–6 eV energy range are due to three core-excited shape resonances as shown in Table II. The Born correction is quite significant for this strong dipole-allowed transition.

The cross sections for exciting the $C\ ^2A_2$, $^4A_2$, and $^4B_2$ states are shown in Fig. 8. In the $X\ ^2A_1 \rightarrow C\ ^2A_2$ transition, the sharp rise at 5.57 eV is due to a core-excited shape resonance of $^1A_1$ symmetry and at 8.34 eV is due to a $^1B_2$ symmetry resonance. In the $X\ ^2A_1 \rightarrow {}^4B_2$ transition, the peak at 5.1 eV is due to a core-excited shape resonance of $^3B_2$ symmetry and sharp rise in cross sections around 10 eV is again due to $^{1,3}A_2$ resonances as shown in Table II. The $X\ ^2A_1 \rightarrow {}^4A_2$ transition shows features near 5.32, 9.1, and 9.8 eV which again correlate with core-excited shape resonances. We have detected many core-excited shape resonances as there are lots of valence states arising due to overlap of atomic orbitals of N and O atoms which are neighbors in the periodic table.

C. Differential cross sections

The DCS provides a more stringent test for any theoretical model than the integrated cross section. We have computed DCS for elastic scattering of NO_2 by electron impact in the energy range of 1–10 eV. The DCS are calculated by processing K matrices using the program POLYDCS [31]. These cross sections are calculated in the fixed nuclei approximation which is equivalent to the summation of rotationally elastic (0-0) and rotationally inelastic (0-J') cross sections for any initial rotor state (we show our results for the $J=0$ level) in the limit of infinitely heavy nuclei [32]. The rotational levels and their eigenfunctions were calculated using the program ASYMTOP [33]. The NO_2 molecule is an asymmetric top with the rotational constants $A=0.979\,638\,2$ meV, $B=0.054\,106\,7$ meV and $C=0.051\,274\,7$ meV. The rotational levels $|J\tau\rangle$ are given in Table III.

TABLE III. Rotational energy levels of NO_2.

J	τ	Energy (meV)
0	0	0.0000
	−1	0.1054
1	0	1.0309
	1	1.0337
	−2	0.3161
	−1	1.2388
2	0	1.2473
	1	4.0239
	2	4.0239
	−3	0.6323
	−2	1.5507
	−1	1.5677
3	0	4.3401
	1	4.3401
	2	8.9749
	3	8.9749
	−4	1.0537
	−3	1.9666
	−2	1.9949
	−1	4.7616
4	0	4.7617
	1	9.3963
	2	9.3963
	3	15.885
	4	15.885
	−5	1.5805
	−4	2.4864
	−3	2.5289
	−2	5.2885
	−1	5.2887
5	0	9.9233
	1	9.9233
	2	16.412
	3	16.412
	4	24.755
	5	24.755

Figure 9 shows our calculated DCS at 1, 2, 5, and 10 eV in our R-matrix model that included 21 states as enumerated in Table I. These energies are chosen since they are off from the resonance positions. The DCS are obtained by summing over DCS for all rotational cross sections $00 \rightarrow J'\tau'$ with $J'=0$, 1, 2, 3, 4, and 5. The large cross sections in the forward direction are due to the dipolar nature of the target. As yet there is no experimental or theoretical DCS available for comparison.

The state-resolved cross sections at 4 eV are shown in Fig. 10. The contribution of rotationally elastic $(0 \rightarrow 0)$ and rotationally inelastic $(0 \rightarrow J';\ J'=1,\ldots,5)$ transitions is shown. Since NO_2 is a weakly polar molecule, the $0 \rightarrow 1$ contribution is much smaller than the elastic $0 \rightarrow 0$ compo-

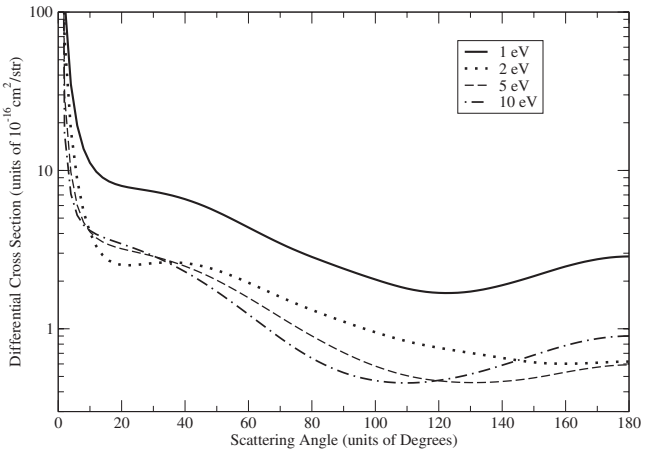

FIG. 9. Differential elastic cross section at different energies: solid curve, 1 eV; dotted curve, 2 eV; dashed curve, 5 eV; and dotted-dashed curve, 10 eV.

nent except at very low angles. The elastic component is therefore the dominant feature of the state-resolved DCS. As J' increases, the contribution due to $J'>2$ decreases dramatically showing that our DCS are converged with respect to J'. The rather flat curve for $0\rightarrow 2$ component reflects the fact that it is due to the quadrupole moment of the molecule which in the Born approximation yields a constant value $(0.25\ \text{Å}^2)\ (4/45)Q^2$, where Q is the quadrupole moment of NO_2 ground state at its equilibrium geometry whose value is 3.17 a.u. in R-matrix method. In Fig. 10, the cross sections are summed over τ'.

Figure 11 shows the momentum transfer cross sections (MTCSs) which are sensitive to backward scattering. The undulations in the MTCS are due to the effect of resonances. At energy below 2 eV, the cross sections increase rapidly as energy decreases. At the higher end of energy range, the MTCS tend to be rather flat.

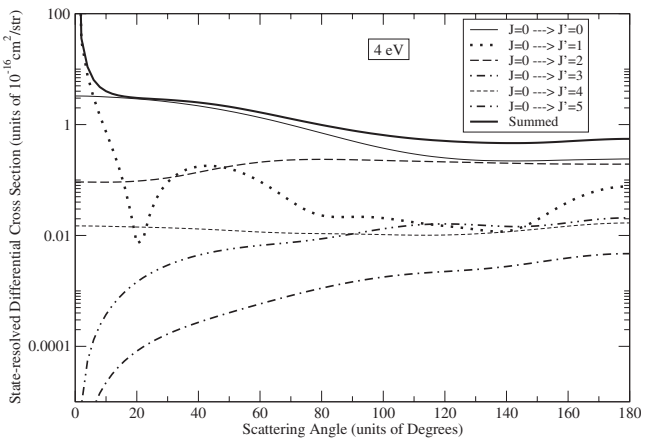

FIG. 10. State-resolved DCS (summed over τ)at 4 eV: thin solid curve, $J=0\rightarrow J'=0$; dotted curve, $J=0\rightarrow J'=1$; thick dashed curve, $J=0\rightarrow J'=2$; dashed-dotted curve, $J=0\rightarrow J'=3$; thin dashed curve, $J=0\rightarrow J'=4$; and dotted-dashed curve, $J=0\rightarrow J'=5$. For all J', the sum is over all values of τ'. Thick solid curve, summation of all transitions mentioned.

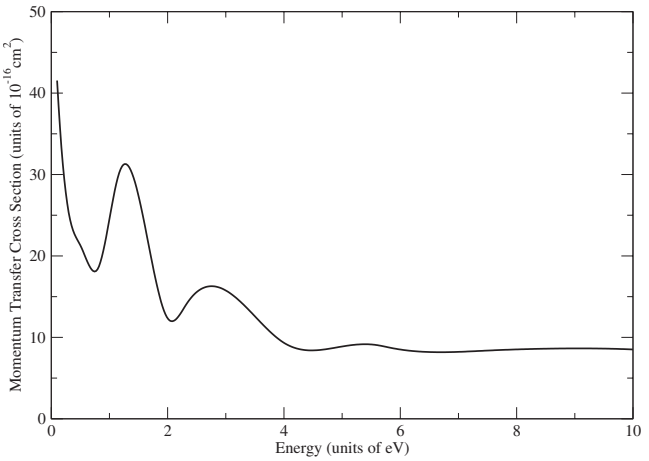

FIG. 11. Momentum transfer cross section for energy range of 0–10 eV.

VI. VARIATION OF RESONANT STATES WITH GEOMETRY

The present study identifies the presence of two low-lying shape resonances of B_1 symmetry. To explore the possible dissociative nature of these resonant states, we have investigated their dependence on geometry by performing calculations in which one N-O bond and the ONO angle are fixed at their equilibrium values and the other N-O bond is stretched from its equilibrium value to $3a_o$.

The calculations are performed in C_s point group, in which A' symmetry correlates with A_1 and B_2 symmetries of C_{2v} point group and the other A'' symmetry of C_s correlates with the other two symmetries of C_{2v} point group. Both shape resonances are thus explored via A'' symmetry only.

Figure 12 shows the positions and the widths of the A'' resonances as a function of the resonant positions and widths of $^3A''$ ($^3B_1$) and $^1A''$ ($^1B_1$) states approaches zero around $2.5a_o$ and $2.7a_o$, respectively. Thus both the states support dissociative attachment. Since we have stretched only one O atom along one particular N-O bond, the scattering electron

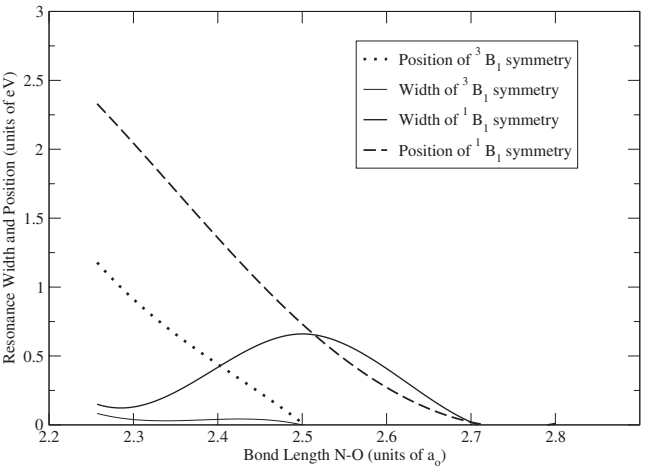

FIG. 12. Variation of resonance width and position with bond length: dotted curve, position of $^3B_1$; thin solid curve, width of $^3B_1$; thick solid curve, width of $^1B_1$; and dashed curve, position of $^1B_1$.

in this stretching mode can only attach itself to O atom and NO molecule. Assuming that the products remain in their ground states, there are only two possible two-body fragmented channels:

$$NO_2^-(^1A_1, ^{1,3}B_1) \rightarrow NO(X\ ^2\Pi) + O^-(^2P),$$

$$NO_2^-(^3B_1) \rightarrow NO^-(X\ ^3\Sigma^-) + O(^3P).$$

The first channel correlates to three low-lying states $^1A_1$, $^1B_1$, and $^3B_1$ of NO_2^-. The second channel correlates to $^3B_1$ state. The $^1A_1$ state is not formed by electron impact because its potential-energy curve lies lower than the $^2A_1$ potential curve of NO_2 in the Franck-Condon region [13]. Since we have detected shape resonances in $^1B_1$ and $^3B_1$ symmetries, we assign the first channel to $^1B_1$ state of NO_2^-.

VII. CONCLUSIONS

This is a detailed study of electron impact excitation of the NO_2 radical. Our calculation shows the presence of two low-lying shape resonances of B_1 symmetry and one shape resonance of A_1 symmetry at higher energy. The average position of shape resonances of $^1B_1$ and $^3B_1$ symmetries is well correlated for the appearance of an O^- peak in the dissociative electron attachment spectra of NO_2 molecule. Our *R*-matrix calculations also predict one Feshbach and eight core-excited shape resonances of different symmetries. We find fair agreement between our *R*-matrix results with the SCE calculations [15] for each symmetry component. Our results for the total cross sections are in good agreement with the experimental results [14] for scattering energies above 5 eV. We also present differential cross sections at selected energies which can be compared with any future experimental study. State-resolved cross sections at 4 eV reveal that, since NO_2 is a weakly polar molecule, the main contribution is due to the elastic component $0 \rightarrow 0$. The momentum transfer cross sections provided here may aid the study of swarm experiments for electron drifting in the gaseous NO_2 molecule.

ACKNOWLEDGMENTS

This work was financially supported by Council of Scientific and Industrial Research (CSIR), India under Grant No. F.NO. 2-56/2002(I)EU.II. We are also grateful to Royal Society London and British Council (India) for providing funds under India-UK Exchange Programme.

[1] I. M. Campbell, *Energy and the Atmosphere* (Wiley, New York, 1977).
[2] G. D. Gillispie, A. U. Khan, A. C. Wahl, R. P. Hostney, and M. Krauss, J. Chem. Phys. **63**, 3425 (1975).
[3] C. F. Jackels and E. R. Davidson, J. Chem. Phys. **64**, 2908 (1976).
[4] T. D. Crawford, J. F. Stanton, P. G. Szalay, and H. F. Schaefer, J. Chem. Phys. **107**, 2525 (1997).
[5] J. Lievin, A. Delon, and R. Jost, J. Chem. Phys. **108**, 8931 (1998).
[6] V. H. Dibeler, J. A. Walker, and S. K. Liston, J. Res. Natl. Bur. Stand. **71A**, 371 (1967).
[7] P. C. Killgoar, Jr., G. E. Leroi, W. A. Chupka, and J. Berkowitz, J. Chem. Phys. **59**, 1370 (1973).
[8] S. Katsumata, H. Shiromaru, K. Mitani, S. Iwata, and K. Kimura, Chem. Phys. **69**, 423 (1982).
[9] K. Stephan, H. Helm, Y. B. Kim, G. Seykara, J. Ramler, M. Grössl, E. Märk, and T. Mark, J. Chem. Phys. **73**, 303 (1980).
[10] C. Benoit and R. Abouaf, Chem. Phys. Lett. **177**, 573 (1991).
[11] R. E. Fox, J. Chem. Phys. **32**, 285 (1960).
[12] J. A. D. Stockdale, R. N. Compton, G. S. Hurst, and P. W. Reinhardt, J. Chem. Phys. **50**, 2176 (1969).
[13] R. Abouaf, R. Paineau, and F. Fiquet-Fayard, J. Phys. B **9**, 303 (1976).
[14] C. Szmytkowski, K. Maciag, and A. M. Krzysztofowicz, Chem. Phys. Lett. **190**, 141 (1992).
[15] R. Curik, F. A. Gianturco, R. R. Lucchese, and N. Sanna, J. Phys. B **34**, 59 (2001).
[16] L. A. Morgan, C. J. Gillan, J. Tennyson, and X. Chen, J. Phys. B **30**, 4087 (1997).
[17] L. A. Morgan, J. Tennyson, and C. J. Gillan, Comput. Phys. Commun. **114**, 120 (1998).
[18] J. Tennyson, J. Phys. B **29**, 1817 (1996).
[19] B. M. Nestmann, K. Pfingst, and S. D. Peyerimhoff, J. Phys. B **27**, 2297 (1994).
[20] T. H. Dunning and P. J. Hay, *Methods of Electronic Structure Theory* (Plenum, New York, 1977), Vol. 2.
[21] E. Leonardi, C. Petrongolo, G. Hirsch, and R. J. Buenker, J. Chem. Phys. **105**, 9051 (1996).
[22] K. M. Ervin, J. Ho, and W. C. Lineberger, J. Phys. Chem. **92**, 5405 (1988).
[23] A. Faure, J. D. Gorfinkiel, L. A. Morgan, and J. Tennyson, Comput. Phys. Commun. **144**, 224 (2002).
[24] F. A. Gianturco and R. R. Lucchese, J. Chem. Phys. **111**, 6769 (1999).
[25] F. A. Gianturco, A. Jain, and L. C. Pantano, J. Phys. B **20**, 571 (1987).
[26] J. P. Perdew and A. Zunger, Phys. Rev. B **23**, 5048 (1981).
[27] J. Tennyson and C. J. Noble, Comput. Phys. Commun. **33**, 421 (1984).
[28] S. A. Rangwala, E. Krishnakumar, and S. V. K. Kumar, in *21st International Conference on Physics of Electronic and Atomic Collisions, Sendai, 1999*, edited by Y. Itikawa *et al.*, p. 324.
[29] A. Faure, J. D. Gorfinkiel, and J. Tennyson, J. Phys. B **37**, 801 (2004).
[30] S. Kaur, K. L. Baluja, and J. Tennyson, Phys. Rev. A **77**, 032718 (2008).
[31] N. Sanna and F. A. Gianturco, Comput. Phys. Commun. **114**, 142 (1998).
[32] E. S. Chang and A. Temkin, Phys. Rev. Lett. **23**, 399 (1969).
[33] A. Jain and D. G. Thompson, Comput. Phys. Commun. **30**, 301 (1983).